LBL-29515
Preprint

Lawrence Berkeley Laboratory
UNIVERSITY OF CALIFORNIA

Materials & Chemical Sciences Division

Submitted to the Journal of the American Ceramic Society

Cyclic Fatigue Life and Crack-Growth Behavior of Microstructurally-Small Cracks in Mg-PSZ Ceramics

A.A. Steffen, R.H. Dauskardt, and R.O. Ritchie

August 1990

LOAN COPY
Circulates
for 4 weeks
Bldg. 50 Library.
Copy 2
LBL-29515

Prepared for the U.S. Department of Energy under Contract Number DE-AC03-76SF00098

DISCLAIMER

This document was prepared as an account of work sponsored by the United States Government. While this document is believed to contain correct information, neither the United States Government nor any agency thereof, nor the Regents of the University of California, nor any of their employees, makes any warranty, express or implied, or assumes any legal responsibility for the accuracy, completeness, or usefulness of any information, apparatus, product, or process disclosed, or represents that its use would not infringe privately owned rights. Reference herein to any specific commercial product, process, or service by its trade name, trademark, manufacturer, or otherwise, does not necessarily constitute or imply its endorsement, recommendation, or favoring by the United States Government or any agency thereof, or the Regents of the University of California. The views and opinions of authors expressed herein do not necessarily state or reflect those of the United States Government or any agency thereof or the Regents of the University of California.

LBL-29515

CYCLIC FATIGUE LIFE AND CRACK-GROWTH BEHAVIOR OF MICROSTRUCTURALLY-SMALL CRACKS IN Mg-PSZ CERAMICS

A. A. Steffen,* R. H. Dauskardt and R. O. Ritchie

Center for Advanced Materials, Lawrence Berkeley Laboratory
and
Department of Materials Science and Mineral Engineering
University of California, Berkeley, CA 94720

*currently with Failure Analysis Associates, Menlo Park, CA 94025

August 1990

submitted to the *Journal of American Ceramic Society*

Work supported by the Director, Office of Energy Research, Office of Basic Energy Sciences, Materials Sciences Division of the U.S. Department Energy under Contract No. DE-AC03-76SF00098.

CYCLIC FATIGUE LIFE AND CRACK-GROWTH BEHAVIOR OF MICROSTRUCTURALLY-SMALL CRACKS IN Mg-PSZ CERAMICS

A. A. Steffen,* R. H. Dauskardt and R. O. Ritchie

Center for Advanced Materials, Lawrence Berkeley Laboratory
and
Department of Materials Science and Mineral Engineering
University of California, Berkeley, CA 94720

Cyclic fatigue stress/life (S/N) and crack-growth properties are investigated in magnesia partially-stabilized zirconia (Mg-PSZ), with particular reference to the role of crack size. The material studied was subeutectoid aged to vary the steady-state fracture toughness K_c from ~3 to 16 MPa$\sqrt{m}$. S/N data from unnotched specimens show markedly lower lives under tension-compression compared to tension-tension loading; "fatigue limits" (at 10^8 cycles) for the former case approach 50% of the tensile strength. Under tension-tension loading, cyclic crack-growth rates of "long" (>3 mm) cracks are found to be power-law dependent on the stress-intensity range ΔK with a fatigue threshold, ΔK_{TH}, of order 50% K_c. Conversely, naturally-occurring "small" (1 to 100 μm) surface cracks were observed to grow at ΔK levels some 2 to 3 times smaller than ΔK_{TH}, similar to behavior widely reported for metallic materials. The observed small-crack behavior is rationalized in terms of the restricted role of crack-tip shielding (in PSZ from transformation toughening) with cracks of limited wake, analogous to the reduced role of crack closure with small fatigue cracks in metals. The implications of such data for structural design with ceramics are briefly discussed.

*currently with Failure Analysis Associates, Menlo Park, CA 94025.

I. Introduction

Recently, there has been increasing concern over the apparently anomalous behavior of "small" fatigue cracks in the engineering design and life prediction of structures (e.g., 1). Where cracks are physically small (typically of a length less than ~500 μm) or approach the dimensions of microstructure or local crack-tip inelasticity, crack propagation rates are known to exceed those of "long" cracks (typically in excess of ~3 mm) at equivalent applied stress-intensity ranges ΔK, and more importantly to occur at ΔK levels *less than* the fatigue threshold ΔK_{TH}, below which fatigue cracks are presumed dormant. Since fracture-mechanics based (damage-tolerant) design and life-prediction procedures invariably utilize conventional long-crack data and generally preclude such early crack growth, the accelerated and *sub-threshold* growth of small cracks provides a strong potential for non-conservative prediction.

The various classes of small cracks have been identified for metallic materials and are reproduced in Table I (2). In a broader context, the small-crack effect primarily arises from the restricted influence of crack-tip shielding* mechanisms in cracks of limited wake (1,2,4). Here, "small" is best defined as comparable in size to the equilibrium or steady-state extent of shielding which is most often developed *behind* the crack tip. The principal mechanism of such shielding in metal fatigue is generally crack closure, i.e., premature contact between crack surfaces during the unloading cycle due, for example, to wedging from fracture-surface asperities or corrosion debris (5,6). Accordingly, at a given applied stress intensity, a small crack may experience a larger *local* (near-tip) "driving force" than an equivalent long crack due to less wake shielding, analogous to the resistance-curve (R-curve) phenomenon in toughness tests.

Indeed, any pertubation of the steady-state shielding or toughening mechanism may lead to non-unique values of the crack-tip stress intensity even for long cracks. During processes of subcritical cracking, for example, environmentally enhanced or cyclically induced crack growth, this may result in abnormal crack-growth velocities until steady-state shielding is re-established. Such transient subcritical crack-growth behavior following abrupt applied load changes has been reported for a transformation-

*Crack-tip shielding mechanisms act to impede crack advance by lowering the local stress intensity actually experienced at the crack tip (3,4). Such mechanisms, which act principally in the crack wake, include transformation and microcrack toughening in ceramics, crack bridging in composites, and crack closure during fatigue-crack growth.

TABLE I - Classes of Small Fatigue Cracks (2)

Type of Small Crack	Dimension	Responsible Mechanism
Mechanically small	$a \lesssim r_y$ +	Excessive (active) plasticity
Microstructurally small	$a \lesssim d_g$ ++	Crack-tip shielding, enhanced local plastic strain
	$2c \lesssim (5\text{-}10)\ d_g$	Crack shape
Physically small	$a \lesssim 1$ mm	Crack-tip shielding (crack closure)
Chemically small	Up to about 10 mm +++	Local crack-tip environment

+ r_y is the plastic zone size or plastic field of notch.
++ d_g is the critical microstructural dimension, e.g., grain size, a is the crack depth and 2c the surface length.
+++ Critical size is a function of frequency and reaction kinetics.

toughened Mg-PSZ ceramic (7). Theoretical analysis of the extent of the post load-change crack-tip shielding from transformation toughening allowed fairly accurate prediction of the transient crack-growth behavior.

Since many advanced ceramic materials are toughened by shielding mechanisms (3), e.g., transformation toughening or fiber/whisker bridging, small-crack effects are expected to be significant. In fact, fracture-toughness tests on transformation-toughened Mg-PSZ show R-curves for small (< 400 μm) surface cracks to occur at lower applied K levels than those for long cracks (8). Moreover, for subcritical cracking under monotonic loads, results for ~100 μm long cracks growing out of residual stress fields around hardness indents in soda-lime glass (9), and ~20-200 μm long surface cracks in bend specimens of Mg-PSZ (10), both show sub-threshold crack-growth behavior with a negative dependency on applied K, akin to behavior in metals (1). Similarly for fatigue, small-crack data have been reported for surface cracks (< 300 μm) in Ce-PSZ (11), for indentation cracks (< 50 μm) in Al_2O_3 and Si_3N_4 (12), and for corner cracks (< 250 μm) in LAS/SiC-fiber glass-ceramics (13). Although growth rates in the latter three ceramics all show a negative dependency on K, no comparisons have been made with long-crack fatigue data in the same material.

The objective of the present study is to investigate the cyclic fatigue behavior of a well characterized ceramic, Mg-PSZ, with reference to the role of microstructurally-small cracks. Fatigue properties are examined in terms of classical stress/life (S/N) and crack-propagation rate data; in the latter case results are compared for long pre-existing through-thickness cracks with naturally-occurring small surface cracks.

II. Experimental Procedures

(1) Material

The material examined was a partially-stabilized zirconia, containing 9 mol% magnesia (Mg-PSZ),* chosen for its well characterized and controllable transformation-toughening behavior (14-16). Sintering and heat treatment in the cubic phase field, followed by controlled cooling and subeutectoid aging at 1100°C for 3 to 24 h, resulted in a series of microstructures consisting of cubic ZrO_2 grains (diameter ~50 μm), with ~35-40 vol% lens-shaped tetragonal precipitates (maximum size ~300 nm). The tetragonal precipitates undergo a stress-induced martensitic transformation to a monoclinic phase in the high stress field near the crack tip. The resultant dilatant transformation zone in the wake of the crack exerts compressive tractions on the crack surfaces and shields the crack tip from the applied (far-field) stresses (see for example, 17,18). The crack-tip stress intensity, K_{tip}, is therefore reduced from the applied (far-field) K by an amount, K_s, such that:

$$K_{tip} = K - K_s \,, \tag{1}$$

where the shielding stress intensity K_s is dependent upon the volume fraction, f, of the transforming phase within the zone, the width of the zone, and the dilatational component of the transformation strain ε^T. The value of K_s increases with initial crack extension producing the well known resistance-curve behavior until a steady-state condition is achieved after distances approximately 5 times the transformation zone width, w, where (17):

$$K_s = A\, E'\, \varepsilon^T\, f\, w^{\frac{1}{2}} \,, \tag{2}$$

with $E' = E/(1 - \nu^2)$, E is Young's modulus, ν is Poisson's modulus, and the constant A is dependent upon the frontal zone shape. Direct observations of the transformation zones in Mg-PSZ suggest that the zone shape is approximately semicircular ahead of the crack tip for which A = 0.25 (19).

The specific microstructures examined and their room-temperature properties are listed in Table II; these structures vary from the peak toughened (TS-grade) condition (steady-state K_c ~ 17 MPa$\sqrt{m}$) to an overaged (non-transformation-toughened) condition (K_c ~ 3 MPa$\sqrt{m}$).

---

*Nilcra Ceramics, Northcote, Australia.

TABLE II - Heat Treatments and Tensile Properties of Mg-PSZ

Condition (grade)	Heat Treatment	Young's Modulus, E (GPa)	Approx. Tensile Strength (MPa)	Fracture Toughness† K_i (MPa√m)	K_c
overaged	24 h at 1100°C	<200	300	2.5	2.9
low toughness (AF)	as received	208	300	3.0	5.5
mid toughness (MS)	3 h at 1100°C	208	600	3.0	11.5
peak toughness (TS)	7 h at 1100°C	208	400	4.0	16.9

†K_i and K_c are the initiation and plateau toughness values from R-curves obtained from indentation small-crack and C(T) long-crack experiments, respectively.

(2) Stress/Life (S/N) Testing

S/N fatigue tests were performed on unnotched cantilever-bend specimens (9 mm wide, 5 mm thick and 70 mm long), with surfaces polished to ~1 μm finish (Fig. 1a). Specimens were cycled for up to 10^8 cycles under tension-compression (stress ratio $R = \sigma_{min}/\sigma_{max} = -1$) and tension-tension ($R = 0$) loading in controlled ambient-temperature air (22°C, 45% relative humidity) at a nominal sinusoidal frequency of 100 Hz in a variable-speed, constant-displacement testing machine. Data are presented as number of cycles to failure, N_f, as a function of the maximum applied stress, σ_{max}, computed from the remote (outer surface) bending stress.

(3) Crack-Propagation Testing: Small Cracks

Fracture-mechanics fatigue-crack propagation data for naturally-occurring small (<100 μm) surface cracks were determined by monitoring the top surface of the cantilever-bend specimens used in the S/N tests. Specimens were periodically removed from the test fixture and optically examined using Nomarski interference microscopy. Tests were interrupted after ~100 cycles to determine damage accumulation during initial loading and after subsequent 10^2 to 10^3 cycle intervals until failure. Small-crack lengths could be readily quantified with a resolution better than ± 0.5 μm, by digitizing optical micrographs of the specimen surface using an image analyzer. Owing to crack meandering, surface crack lengths were taken as the projected crack length normal to the direction of the bending stress. Crack-growth rates were determined over the range 10^{-12} to 10^{-6} m/cycle from crack length/number of cycles (a vs. N) curves. Far-field

stress-intensity factors were computed from linear-elastic solutions* (20,21) for three-dimensional semi-elliptical surface cracks in bending (and/or tension) in terms of crack depth, a, crack length, c, elliptical parametric angle, ϕ, shape factor, Q, specimen width, t, specimen thickness, b, and remote (outer surface) bending stress, σ_b:

$$K = H_c \sigma_b (\pi a/Q)^{\frac{1}{2}} F(a/c, a/t, c/b, \phi) \tag{3}$$

where H_c is the bending multiplier and F is a boundary correction factor (Fig. 1b). Eq. (3) is valid for $0.2 \leq a/c \leq 1$, $0 \leq \phi \leq 90°$ at $c/b \leq 0.5$. Based on optical examination of the morphology of typical small cracks which were chemically stained prior to final fracture of the specimen, a/c ratios were found to be of the order of 0.8. Cyclic crack-growth rates (da/dN) are presented in terms of the maximum stress intensity, K_{max}, from the tensile portion of the fatigue cycle, calculated with a/c = 0.8 at $\phi = 0°$. Note that while many microcracks develop, their mean spacing, particularly during early stages of crack growth, is generally a large multiple of the microcrack length; interaction effects are thus minimal.

(4) Crack-Propagation Testing: Long Cracks

Cyclic fatigue-crack propagation studies for long (>3 mm) cracks were performed on 3-mm thick compact C(T) specimens containing through-thickness cracks, which were cycled at R = 0.1 with a sinusoidal frequency of 50 Hz; more details have been presented elsewhere (22-24). Crack initiation was facilitated through the use of a wedge-shaped starter notch. Crack-growth rates, over the range $\sim 10^{-11}$ to 10^{-5} m/cycle were determined under computer-controlled K-decreasing and K-increasing conditions, with a normalized K gradient set at $0.08 mm^{-1}$. An electrical-resistance technique was employed to monitor continuously crack length (with a resolution better than 5 μm) using ~0.1-μm NiCr films, evaporated onto the specimen surface (25).

Cyclic crack-growth rate data are presented in terms of the maximum and alternating stress intensities, K_{max} and ΔK (= K_{max} - K_{min}) respectively, applied during the fatigue cycle. At the completion of these tests, fracture-toughness values were measured from $K_R(\Delta a)$ resistance curves by monotonically loading the C(T) specimens to failure, and measuring the extent of crack extension (Δa). Toughness

*While anisotropy of mechanical properties and residual stress effects at the microstructural level may well limit the application of linear-elastic theory for small cracks, inelastic-zone sizes remain small compared to test piece dimensions. Moreover, the prevailing notion in current analyses of transformation toughening (17,18) is that material near the crack tip, having essentially exhausted its capacity to transform, behaves linear elastically.

values, quoted in Table I, were determined both at crack initiation (K_i) and at the steady-state plateau of the R-curve (K_c).

III. Results and Discussion

(1) S/N Fatigue

S/N curves, derived from results on cantilever-bend specimens of the overaged and MS-grade material, are shown in Fig. 2 for both tension-compression (R = -1) and tension-tension (R = 0) loading. Results of Swain and co-workers (26,27) for Mg-PSZ (Nilcra MS-grade), tested in both low-cycle (flexural) four-point bending (R = 0 and 0.86, frequency 0.03-0.16 Hz) and high-cycle rotating bending (R = -1, frequency 100 Hz) are included for comparison. Despite the obvious scatter, the results at both R ratios are comparable with the present data.

Cycling in tension-compression is clearly more damaging, resulting in reduced lifetimes compared to cyclic tension loading (Fig. 2), similar to previous observations in PSZ (26) and Si_3N_4 (28,29). The MS-grade material appears to show evidence of a "fatigue limit" of approximately 300 MPa (at 10^8 cycles with R = -1); similar to classical behavior of steels, this is roughly 50% of the tensile strength. At comparable stress levels, lives in the overaged material are considerably shorter.

Optical micrographic examination of the specimen surfaces revealed a relatively large number of microcracks (Fig. 3), which were observed to increase in both size and surface density with increasing alternating stress level or number of cycles. The microcrack damage can be highlighted using Nomarski interference which indicates out-of-plane surface distortions, caused by tetragonal-to-monoclinic transformation in highly stressed regions along the specimen surface. Microcracks appear in some but not all regions of surface uplift on the surface of the specimens; their alignment is primarily orthogonal to the stress axis, however, particularly under tension-compression loading, some form at angles up to approximately 45° to the stress axis (Fig. 3). Prior to final failure, these microcracks tend to link up with other cracks generated in similar transformed regions along a line roughly perpendicular to the stress axis (Fig. 4). Localized regions of extensive transformation adjacent to the resulting fracture surface are associated with crack-branching effects.

In addition to the association of regions of transformed material with the occurrence of microcracks mentioned above, microcrack initiation also frequently appeared to be associated with pores on the specimen surface. The occurrence of small (~2.5 μm) naturally-occurring pores together with the equiaxed cubic ZrO_2 grain

structure (diameter ~50μm) was revealed by etching in concentrated HF solution; a representative optical micrograph of the MS-microstructure is presented in Fig. 5. The morphology of a single microcrack after 6900 cycles of tension-compression cycling (maximum stress, σ_{max} = 450 MPa) in the MS microstructure is shown at higher magnification in the sequence of optical micrographs in Fig. 6. Apparent initiation of the microcrack at the pore intersecting the crack was substantiated by examination of the region after 2000 cycles when the crack was small. Apparently, both localized regions of transformed material and naturally occurring pores may be implicated in the nucleation process. Subsequent crack growth was predominantly transgranular as indicated schematically by the dotted line in Fig. 6(c). Note that contrast of the crack may be greatly enhanced by adjustment of the incident light to illuminate only half of the object field (specimen) (Fig. 6(d)) and placement of the crack adjacent to the illuminated region. A similar technique of indirectly illuminating the crack using light scattered from a small restricted region of light has been reported elsewhere (30).

A quantitative indication of the size distribution of microcracks was obtained by employing an image-analysis system. Microcrack distributions following specimen failure, after loading at similar maximum stress levels for tension-compression and tension-tension cycling (σ_{max} = 384 MPa, N_f = 5 x 10^4 cycles, R =-1, and σ_{max} = 374 MPa, N_f = 63 x 10^6 cycles, R = 0) on the surfaces of the MS crack specimens, are shown in Fig. 7. The more damaging nature of tension-compression cycling is clearly apparent from the higher density of larger microcracks observed after cycling at R = -1 compared to R = 0. Corresponding microcrack densities in the overaged condition could not be measured, as instability followed too rapidly following crack initiation.

An indication of the effect of maximum stress level after the same number of cycles at R = -1 on microcrack size distribution was obtained by examining different surface regions along the length of the cantilever beam specimen (Fig. 8). While similar densities of small microcracks ($\lesssim$ 10 μm) were apparent at the low stress (σ_{max} = 252 MPa), mid stress (σ_{max} = 318 MPa), and high stress (σ_{max} = 384 MPa) locations along the cantilever beam, the occurrence of larger microcracks ($\gtrsim$ 30 μm) displayed a marked sensitivity to the maximum applied stress levels. Maximum microcrack lengths were approximately twice as long at the high stress region compared to the low stress region of the specimen (~125 μm and ~60 μm, respectively).

(2) Fatigue-Crack Propagation: Small Cracks

Lengths of selected microcracks at various maximum applied stress levels plotted as a function of (log) number of stress cycles, derived from monitoring the top surface of the cantilever-bend specimens used for the S/N curves, are shown in Fig. 9 for the MS-grade Mg-PSZ at R = -1. The small cracks can be seen to grow at progressively decreasing growth rates with increase in size. Note that this is not immediately apparent in Fig. 9 due to the logarithmic abscessa. However, not all of them arrest; conversely, individual small cracks eventually link up leading to catastrophic failure (Fig. 4). At similar maximum applied stress levels, crack length vs. (log) number of cycles curves are compared for R = 0 and R = -1 loading (Fig. 10). During the initial stages of growth, propagation rates under tension-tension conditions are somewhat slower than in tension-compression; however, after only 20 μm or so of crack extension, growth rates are similar. Since total fatigue lives are invariably longer in tension-tension compared to corresponding tests in tension-compression at the same maximum applied stress, this implies that an additional difference between the two types of loading is in the ease of crack initiation; cracks may be expected to nucleate more readily at R = -1, as shown in Fig. 7, due to the increased shear strain excursions experienced in localized transformed regions.

Using Eq. (3) to compute stress intensities, such data are used to derive plots of crack-propagation rates as a function of K_{max} for individual microcracks, as shown in Fig. 11. Similar to small-crack data reported for Al_2O_3, Si_3N_4 and LAS/SiC_f ceramics (9,12) and behavior in metals (1,2,4), small-crack growth rates display a negative dependency on the applied stress intensity; moreover, they are not a unique function of K_{max} and appear to be sensitive to the level of applied stress. Such characteristic small-crack behavior is discussed further in the following section. Since transformation-induced surface distortions were absent in the overaged condition, small-crack growth data could not be determined for this microstructure due to the difficulty of detecting cracks on the specimen surface.

(3) Fatigue-Crack Propagation: Long Cracks

Corresponding long-crack cyclic fatigue-crack propagation rates* for Mg-PSZ from tension-tension loaded compact specimens are shown in Fig. 12a; data for the MS-grade microstructure are compared with corresponding small-crack results in Fig. 11. As

*Experiments involving monitoring growth rates at constant K_{max} with varying K_{min} have established that such subcritical cracking is a true cyclic fatigue phenomenon (22-24).

discussed elsewhere (22-24), the long-crack data conform to a conventional Paris power-law relationship, as in metals (31):

$$da/dN = C(\Delta K)^m , \tag{4}$$

although the exponent, m, varies between 21 to 42, which is considerably higher than values between 2 and 4 generally found for metals; the constant C also appears to scale inversely with fracture toughness. Similar values of the exponent, m, have been reported for Mg-PSZ by other authors (29,32,33); even higher values have been reported at higher temperatures (33). For each microstructure, an apparent fatigue threshold, ΔK_{TH}, can be defined, below which crack-growth rates are essentially dormant (i.e., below $\sim 10^{-10}$ m/cycle). The value of ΔK_{TH} is approximately 50% K_c, indicating that cyclic crack growth occurs at stress intensities below that required for crack initiation under monotonic loading on the R-curve. It should also be noted that, despite the absence of appreciable transformation "plasticity", the overaged material exhibits fatigue-crack growth behavior with a similar power-law dependency to the toughened conditions.

It is clear from Fig. 12a that with increasing degrees of crack-tip shielding from transformation toughening, resistance to cyclic fatigue-crack extension in Mg-PSZ is increased. In fact, it has been shown that such crack-growth data for the four microstructures can be normalized by characterizing in terms of the near-tip stress-intensity range, ΔK_{tip}, which allows for such transformation shielding (Fig. 12b), viz. (24):

$$\Delta K_{tip} = K_{max} - K_s , \tag{5}$$

where K_s, the shielding stress intensity due to transformation toughening, is computed using the integrated form of Eq. (2) from Raman spectroscopy measurements of the transformation-zone size (34). The increasing slopes of the da/dN vs. applied ΔK data therefore reflect the increasing potency of the transformation shielding contribution in higher toughness materials. When normalized by the toughness, the data fall on a single curve with slope m = 22. An equivalent result can be achieved by normalizing the crack-growth data by $\Delta K/K_c$ (24).

The comparison of the small- and long-crack growth rates in Fig. 11a for the MS-grade microstructure shows the opposite effect, where a diminished role of wake shielding from transformation toughening, in this case from the limited size of the small

cracks, leads to faster crack-growth rates. Akin to behavior in metals (1,2,4,6), small cracks propagate at stress-intensity levels well below the long-crack fatigue threshold (specifically at K_{max} levels of 1.6 MPa$\sqrt{m}$, *a factor of seven less than* K_c), and furthermore grow at progressively decreasing growth rates, i.e., with a negative dependency on stress intensity. Indeed, crack-growth appears to occur at stress intensities even below that of the initiation toughness, K_i, measured from small-crack indentation experiments under monotonic loading. The stress-intensity levels for small-crack growth are, however, comparable to the crack-tip stress intensity levels, ΔK_{tip} (Fig. 12b), estimated from long-crack data.

The sub-threshold crack-growth behavior for small cracks in the Mg-PSZ ceramic can be explained by analogy to small-crack behavior in metals (1,2,4,35). Although the nominal (far-field) stress intensity K increases with increase in crack size, the shielding stress intensity K_s (in metals, resulting primarily from crack closure) is also enhanced as a shielding zone is developed in the crack wake. The near-tip stress intensity (Eq. 1) and hence the crack-growth behavior is thus a result of the mutual competition between these two factors; K_{tip} therefore progressively diminishes until a steady-state shielding zone is established, whereupon behavior approaches that of a long crack. The similarity of the stress-intensity levels for small-crack growth and the calculated near-tip stress-intensity levels for long-crack growth are therefore apparent. In fact, it is clear from Fig. 11b that the initial growth of small cracks occurs at stress-intensity levels typical of the computed data for unshielded long cracks, i.e., the da/dN (ΔK_{tip}) relationship, computed from Eq. 5. In ceramics, such decelerating sub-threshold crack-growth behavior has been modeled in a LAS/SiC_f glass-ceramic, where the predominant shielding resulted from fiber bridging (13); in the present case, however, the shielding results from phase transformation.

Recent analyses of transformation toughening by Stump and Budiansky (36,37) show that the presence of the phase transformation actually promotes the *initiation* of small cracks by reducing the crack-initiation stress. Subsequent transformed regions *ahead* of the tip provide no shielding until the crack advances, whereupon previously transformed material is left in the wake bordering the crack faces, resulting in an increase in K_s. This leads to a decreasing growth rate until a steady-state transformed zone (of a length of the order of five times its forward extent w) is achieved in the crack wake, whereupon long-crack behavior ensues.

VI. Implications

For structural design, the present observations of cyclically-induced small-crack growth in ceramic materials represent a problem. In safety-critical applications involving metallic structures, damage-tolerant approaches are often used which rely on the integration of crack velocity-stress intensity (v/K) curves (e.g., Eq. 4) to estimate the time or number of cycles for a presumed initial defect to grow to failure. Although such cyclic v/K data are now available for many ceramics and ceramic-matrix composites, the approach may prove difficult to utilize in practice because of the large power-law dependence of growth rates (da/dN) on stress intensity, which implies that the estimated life will be proportional to the reciprocal of the applied stress raised to a large power. For example, for a cracked structure subjected to an applied alternating stress $\Delta\sigma$, where the stress-intensity factor K can be defined as:

$$K = Q' \sigma \sqrt{\pi a} , \tag{6}$$

(Q' is a geometry factor and σ is the applied stress), the number of cycles N_f to grow a crack from some initial size a_o to a critical size a_c is given by:

$$N_f \approx \frac{2}{(m-2)\, C(Q'\Delta\sigma)^m \, \pi^{m/2}} \left[a_o^{-(\frac{m-2}{2})} - a_c^{-(\frac{m-2}{2})} \right] , \tag{7}$$

assuming a power-law crack-growth relationship like Eq. 4 (for $m \neq 2$). For a metallic structure where the exponent m is of the order of 2 to 4, a factor of two increase in the applied stress $\Delta\sigma$ depletes the projected life by roughly an order of magnitude; in ceramic structures, conversely, where m values generally exceed 20 and maybe as high as 50 to 100, this same factor of two increase in stress reduces the projected life by some six to thirty orders of magnitude!

The alternative procedure is to redefine the critical crack size in terms of the fatigue threshold ΔK_{TH}, below which crack growth is presumed dormant; this in essence is a crack-initiation criterion where ΔK_{TH} is taken as the effective toughness, rather than the fracture toughness K_c. However, on the basis of the small-crack data generated in the present work (Fig. 11) and elsewhere (9-13), this approach may also be highly non-conservative.

V. Conclusions

Based on a study of the cyclic fatigue properties of overaged and transformation-toughened Mg-PSZ ceramics, involving characterization of fatigue-crack propagation behavior for both long (> 3 mm) and microstructurally-small (< 100 μm) cracks and of stress/life (S/N) curves, the following conclusions can be made:

1. S/N data derived from unnotched cantilever-beam specimens indicate that fatigue lifetimes are significantly shorter in tension-compression (R = -1) compared to tension-tension (R = 0) loading. Similar to steels, at R = -1, the "fatigue limit" at 10^8 cycles approaches 50% of the tensile strength.

2. Cyclic fatigue-crack growth rates for long cracks are found to be power-law dependent on the stress-intensity range, with an exponent between 21 and 42. Slowest growth rates are shown in microstructures with the highest degree of transformation toughening, i.e., with the highest toughness, K_c, although all growth-rate data for Mg-PSZ can be normalized by characterizing in terms of the near-tip stress-intensity range (ΔK_{tip}), which accounts for transformation shielding, or ($\Delta K/K_c$). Values of the (long-crack) fatigue threshold, ΔK_{TH}, approach 50% of K_c.

3. Cyclic fatigue-crack growth rates for naturally-occurring small surface cracks are found to occur at stress-intensity levels significantly smaller than the nominal long-crack threshold ΔK_{TH}; moreover, similar to behavior in metals, small-crack growth rates show a negative dependency on stress intensity and are sensitive to the level of applied stress.

Acknowledgments: This work was supported by the Director, Office of Energy Research, Office of Basic Energy Sciences, Materials Sciences Division of the U.S. Department of Energy under Contract No. DE-ACO3-76SF00098. Thanks are due to Dr. D. B. Marshall of Rockwell International for helpful discussions and for supplying the material, and to David Malone for experimental assistance.

References

1. S. Suresh and R. O. Ritchie, "The Propagation of Short Fatigue Cracks," *Intl. Metals Rev.*, **29** [6] 445-76 (1984).

2. R. O. Ritchie and J. Lankford, "Small Fatigue Cracks: A Statement of the Problem and Potential Solutions," *Mater. Sci. Eng.*, **84**, 11-16 (1986).

3. A. G. Evans, "The New Generation of High Toughness Ceramics," pp. 267-91 in *Fracture Mechanics: Perspectives and Directions (Twentieth Symp.)*, ASTM STP 1020. Edited by R. P. Wei and R. P. Gangloff. American Society for Testing and Materials, Philadelphia, PA, 1989.

4. R. O. Ritchie, "Mechanisms of Fatigue Crack Propagation in Metals, Ceramics and Composites: Role of Crack Tip Shielding," *Mater. Sci. Eng.*, **A103** [1] 15-28 (1988).

5. W. Elber, "The Significance of Fatigue Crack Closure," pp. 230-42 in *Damage Tolerance in Aircraft Structures*, ASTM STP 486. American Society for Testing and Materials, Philadelphia, PA, 1971.

6. S. Suresh and R. O. Ritchie, "Near-Threshold Fatigue Crack Propagation: A Perspective on Fatigue Crack Closure," pp. 227-61 in *Fatigue Crack Growth Threshold Concepts*. Edited by D. L. Davidson and S. Suresh. TMS-AIME, Warrendale, PA, 1984.

7. R. H. Dauskardt, W. C. Carter, D. K. Veirs, and R. O. Ritchie, "Transient Crack-Growth Behavior in Transformation-Toughened Ceramics," *Acta Metall. et Mater.*, **38** [11] 2327-36 (1990).

8. D. B. Marshall and M. V. Swain, "Crack Resistance Curves in Magnesia-Partially-Stabilized Zirconia," *J. Am. Ceram. Soc.*, **71** [6] 399-407 (1988).

9. M. Yoda, "Crack Growth of C(T) Specimens and Indentation Cracks in Glass," *Int. J. Fract.*, **39**, R23-28 (1989).

10. D. Jensen, V. Zelizko, and M. V. Swain, "Small Flaw Static Fatigue Crack Growth in Mg-PSZ," *J. Mater. Sci. Lett.*, **8**, 1154-57 (1989).

11. D. C. Cardona and C. J. Beevers, "Formation and Growth of Short Fatigue Cracks in a Zirconia-Ceria Alloy," *Scripta Metall.*, **23**, 945-50 (1989).

12. T. Hoside, T. Ohara, and T. Yamada, "Fatigue Crack Growth from Indentation Flaw in Ceramics," *Int. J. Fract.*, **37** [1] 47-59 (1988).

13. E. H. Luh, R. H. Dauskardt, and R. O. Ritchie, "Cyclic Fatigue-Crack Growth Behavior of Short Cracks in SiC-Reinforced LAS Glass-Ceramic Composite," *J. Mater. Sci. Lett.*, **9**, 719-25 (1990).

14. R. H. J. Hannick and M. V. Swain, "Magnesia-Partially-Stabilized Zirconia: The Influence of Heat Treatment on Thermomechanical Properties," *J. Aust. Ceram. Soc.*, **18** [2] 53-62 (1982).

15. R. H. J. Hannick, "Microstructural Development of Subeutectoid-Aged ZrO_2 Alloys," *J. Mater. Sci.*, **18** [2] 457-70 (1983).

16. D. B. Marshall, "Strength Characteristics of Transformation Toughened Zirconia," *J. Am. Ceram. Soc.*, **69** [3] 173-80 (1986).

17. R. M. McMeeking and A. G. Evans, "Mechanics of Transformation Toughening in Brittle Materials," *J. Am. Ceram. Soc.*, **65** [5] 242-46 (1982).

18. B. Budiansky, J. W. Hutchinson, and J. C. Lambropoulos, "Continuum Theory of Dilatant Transformation Toughening in Ceramics," *Int. J. Solids Struct.*, **19** [4] 337-55 (1983).

19. D. B. Marshall, M. C. Shaw, R. H. Dauskardt, R. O. Ritchie, M. Readey, and A. H. Heuer, "Crack-Tip Transformation Zones in Toughened Zirconia," *J. Am. Ceram. Soc.*, **73** [9] 2659-66 (1990).

20. J. C. Newman, Jr. and I. S. Raju, "Stress-Intensity Factor Equations for Cracks in Three-Dimensional Finite Bodies Subjected to Tension and Bending Loads," pp. 312-34 in *Computational Methods in the Mechanics of Fracture*, Chapter 9, Vol. 2. Edited by S. N. Atluri. North Holland, Amsterdam, 1986.

21. I. S. Raju, S. N. Atluri, and J. C. Newman, Jr., "Stress Intensity Factors for Small Surface and Corner Cracks," pp. 297-316 in *Fracture Mechanics: Perspectives and Directions (Twentieth Symp.)*, ASTM STP 1020. Edited by R. P. Wei and R. P. Gangloff. American Society for Testing and Materials, Philadelphia, PA, 1989.

22. R. H. Dauskardt, W. Yu, and R. O. Ritchie, "Fatigue Crack Propagation in Transformation-Toughened Zirconia Ceramic," *J. Am. Ceram. Soc.*, **70** [10] C248-52 (1987).

23. R. H. Dauskardt and R. O. Ritchie, "Cyclic Fatigue Behavior in Ceramics," *Closed Loop*, **17** [2] 7-17 (1989).

24. R. H. Dauskardt, D. B. Marshall, and R. O. Ritchie, "Cyclic Fatigue-Crack Propagation in Magnesia-Partially-Stabilized Zirconia Ceramics," *J. Am. Ceram. Soc.*, **73** [4] 893-903 (1990).

25. P. K. Liaw, H. R. Hartmann and W. A. Lodgson, "A New Transducer to Monitor Fatigue Crack Propagation," *J. Test. Eval.*, **11** [3] 202-7 (1983).

26. M. V. Swain and V. Zelizko, "Comparison of Static and Cyclic Fatigue in Mg-PSZ Alloys", pp. 595-606 in *Advances in Ceramics, 24B Science and Technology of Zirconia III*. Edited by S. Somioya, N. Yammoto and H. Hanagida. American Ceramic Society, Westerville, OH, 1988.

27. M. V. Swain, V. Zelinko, S. Lam, and M. Marach, "Comparisons of the Static and Cyclic Fatigue Behaviour of Mg-PSZ and Alumina in Ringer's Solution," in *Biomaterials*, MRS International Meeting on Advanced Materials, Proceedings, Vol. 1. Materials Research Society, Pittsburgh, PA, 1989.

28. T. Kawakubo and K. Komeya, "Static and Cyclic Fatigue Behavior of Sintered Silicon Nitride at Room Temperature," *J. Am. Ceram. Soc.*, **70** [6] 400-5 (1987).

29. M. Masuda, T. Soma, M. Matsui, and I. Oda, "Fatigue of Ceramics (Part 1) - Fatigue Behavior of Sintered Si_3N_4 under Tension-Compression Cyclic Stress", *J. Ceram. Soc. Japn. Int. Ed.*, **96** 275-80 (1988).

30. D. Johnson-Walls, M. D. Drory, A. G. Evans, D. B. Marshall, and K. T. Faber, "Evaluation of Reliability of Brittle Components by Thermal Stress Testing," *J. Am. Ceram. Soc.*, **70**[7] 363-67 (1985).

31. P. C. Paris and F. Erdogan, "A Critical Analysis of Crack Propagation Laws," *J. Bas. Eng.*, Trans. ASME, **85**, 528-34 (1963).

32. L. A. Sylva and S. Suresh, "Crack Growth in Transforming Ceramics under Cyclic Tensile Loads," *J. Mater. Sci.*, **24** [5] 1729-38 (1989).

33. D. L. Davidson, J. B. Campbell, and J. Lankford, "Fatigue Crack Growth through Partially Stabilized Zirconia at Ambient and Elevated Temperatures," *Acta Metall. et Mater.*, **39** (1991), in press.

34. R. H. Dauskardt, D. K. Veirs and R. O. Ritchie, "Spatially Resolved Raman Spectroscopy Study of Transformed Zones in Magnesia-Partially-Stabilized Zirconia," *J. Am. Ceram. Soc.*, **72** [7] 1124-30 (1989).

35. R. O. Ritchie and W. Yu, "Short Crack Effects in Fatigue: A Consequence of Crack Tip Shielding," pp. 167-89 in *Small Fatigue Cracks*. Edited by R. O. Ritchie and J. Lankford. TMS-AIME, Warrendale, PA (1986).

36. D. M. Stump and B. Budiansky, "Crack-Growth Resistance in Transformation-Toughened Ceramics," *Int. J. Solids Structures*, **25** [6] 635-46 (1989).

37. D. M. Stump and B. Budiansky, "Finite Cracks in Transformation-Toughened Ceramics," *Acta. Metall.*, **37** [12] 3297-3304 (1989).

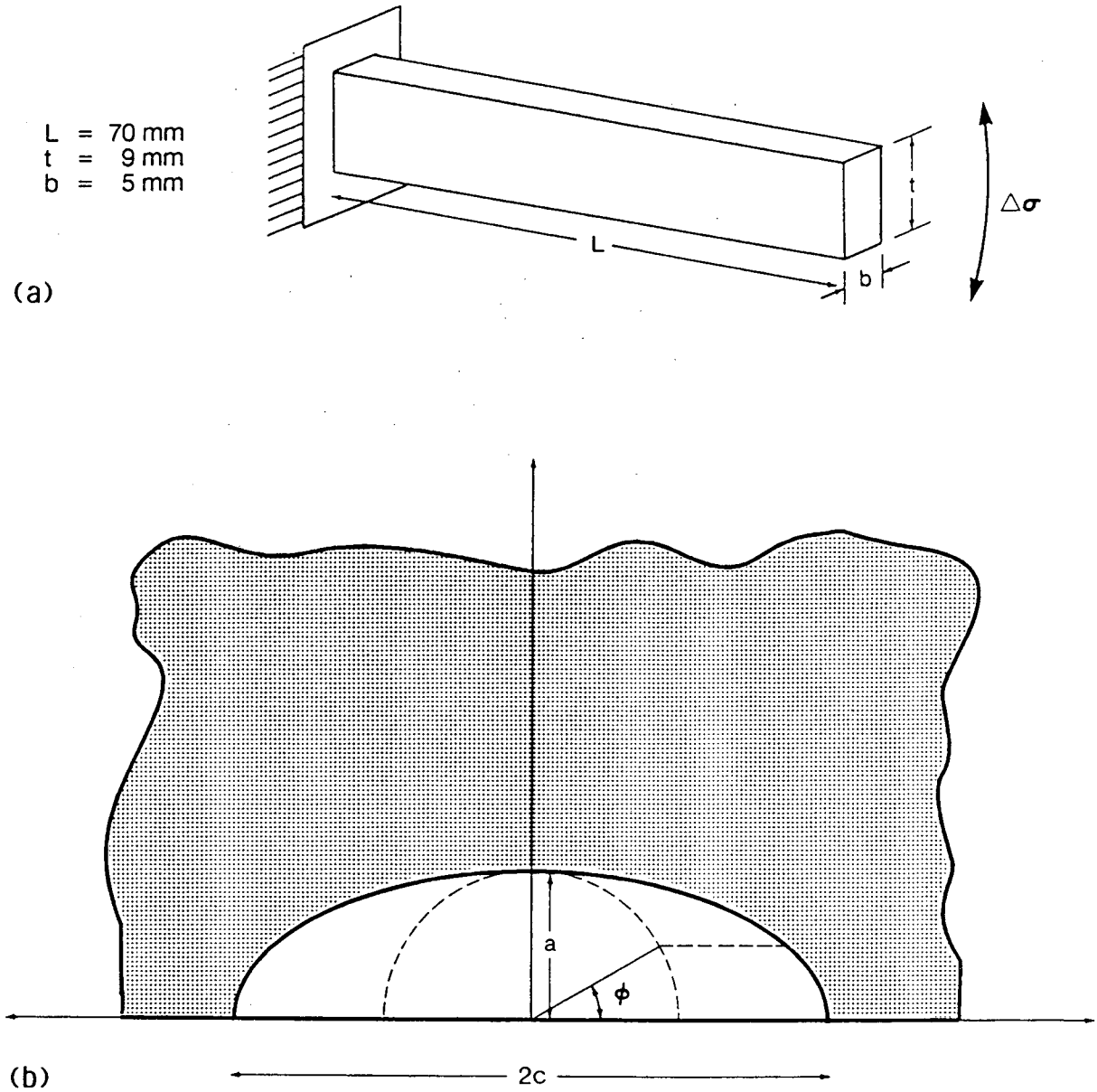

XBL 899-3485B

Fig. 1: Schematic illustration of a) cantilever beam specimen used for S/N and small-crack fatigue tests, and b) semi-elliptical surface crack configuration.

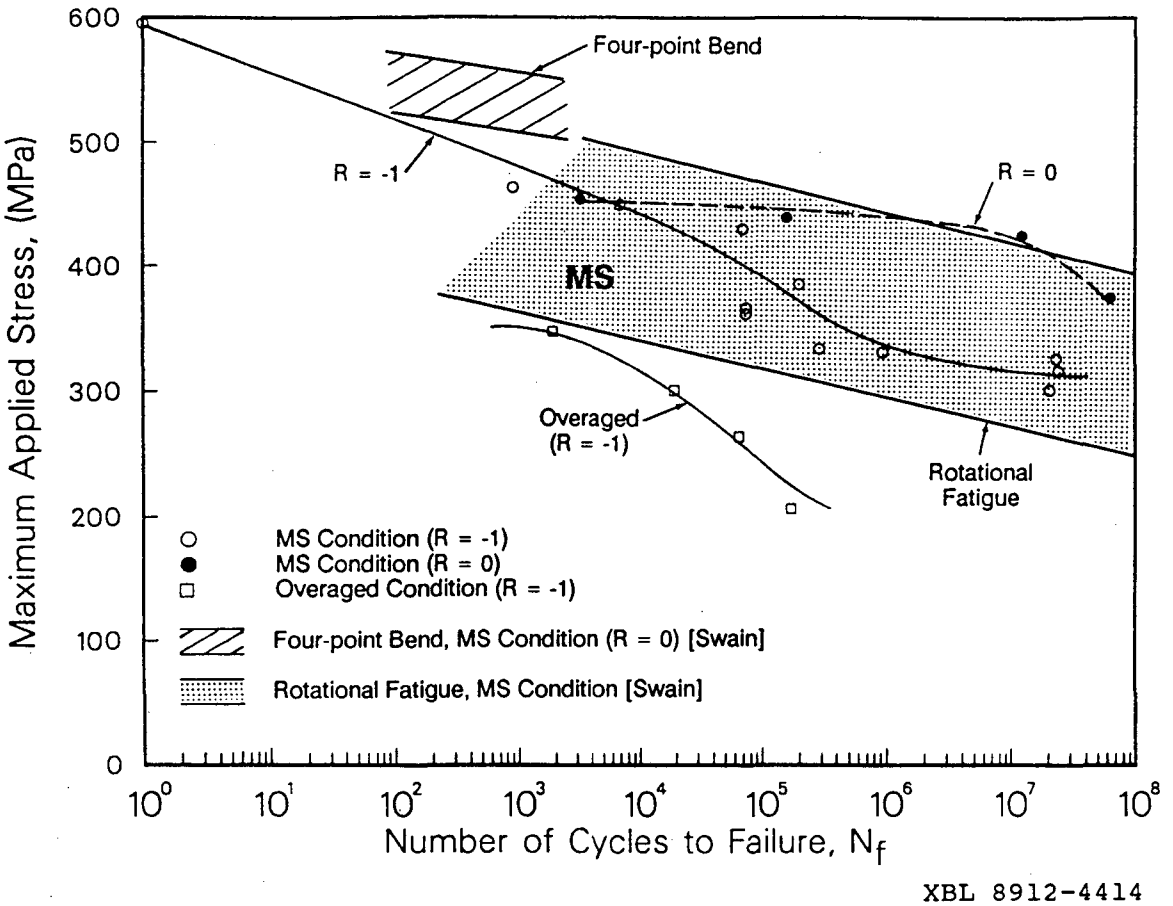

Fig. 2: Stress/life (S/N) curves for the overaged and MS-grade Mg-PSZ, tested in cantilever bend under tension-compression (R = -1) and tension-tension (R = 0) cycling. Data are compared with results of Swain and Zelizko (26) on a similar MS-grade Mg-PSZ material under cyclic flexure (R = 0) and rotating flexure (R = -1).

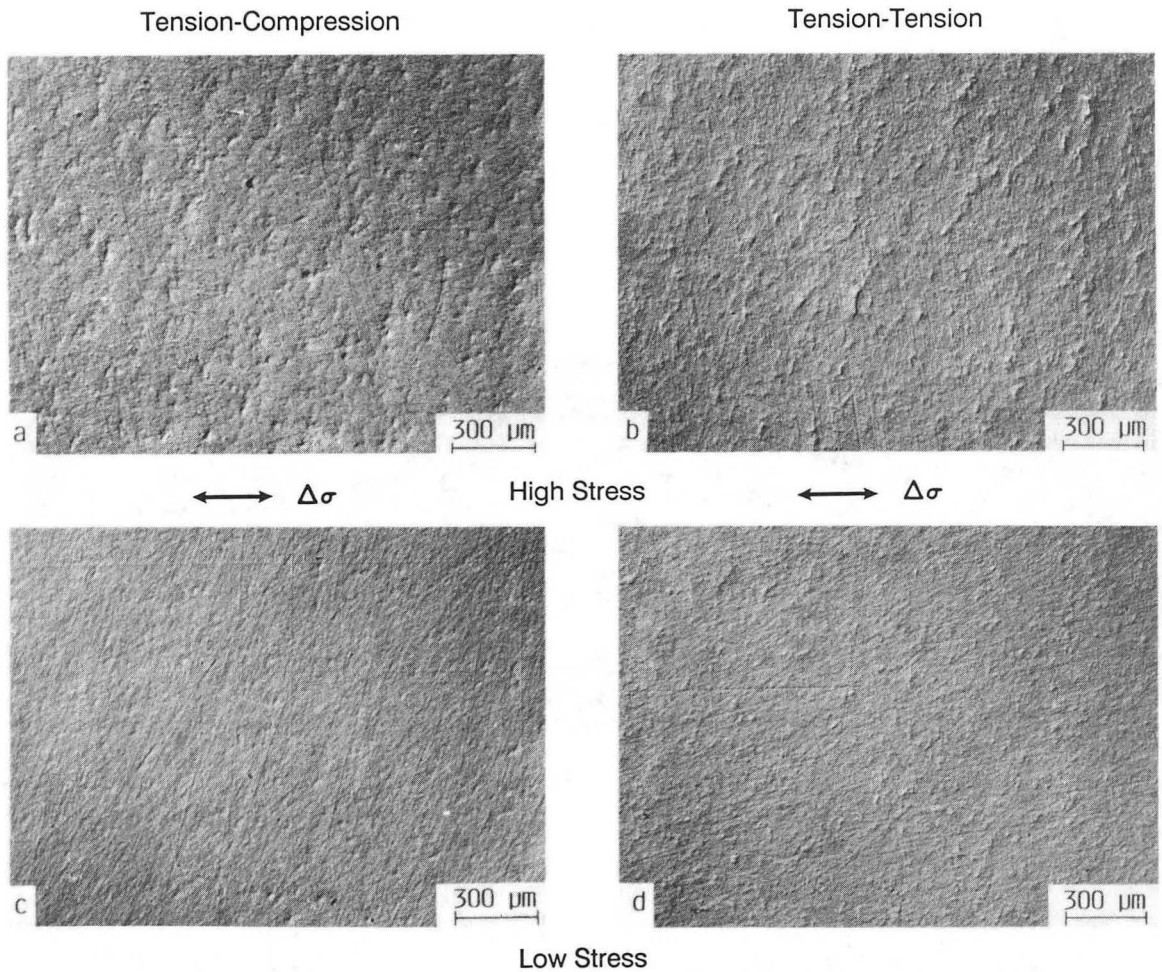

XBB 906-4974A

Fig. 3: Representative optical micrographs using Nomarski interference techniques showing the surface of cantilever-beam specimens cycled to failure in MS-grade Mg-PSZ taken at the high stress (σ_{max} ~ 450 MPa) side of the specimen with (a) R = -1 and (b) R = 0, and at the low stress (σ_{max} ~ 295 MPa) side with (c) R = -1 and (d) R = 0. Microcracks were primarily observed to initiate orthogonal to the stress axis, however, particularly under tension-compression loading, microcracks were apparent at angles up to ~45° to the loading axis.

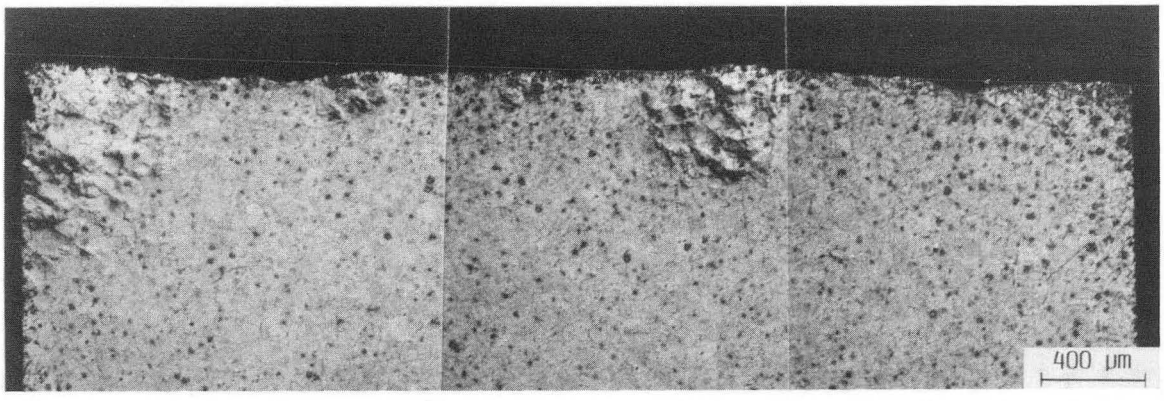

XBB 909-7172

Fig. 4: Optical micrograph of the HF etched surface of a fractured cantilever-beam specimen of MS-grade Mg-PSZ showing the final fracture which results from coalescence of microcracks along a line perpendicular to the stress axis. Regions of intense transformation are associated with crack branching effects.

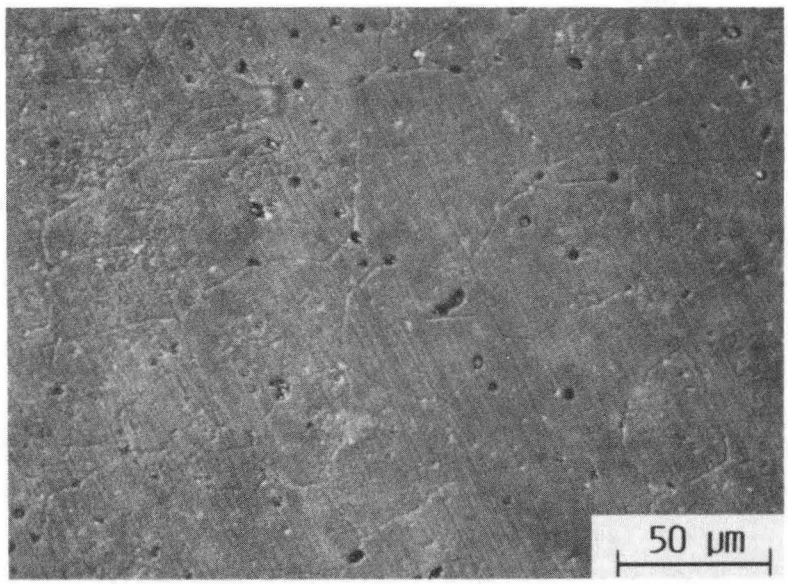

XBB 909-7173

Fig. 5: Typical equiaxed microstructure of the cubic ZrO_2 phase with a grain size of approximately 50 μm revealed by etching for ~3 min in a concentrated HF solution. A dispersion of small pores (~2.5 μm diameter) is also apparent in the micrograph.

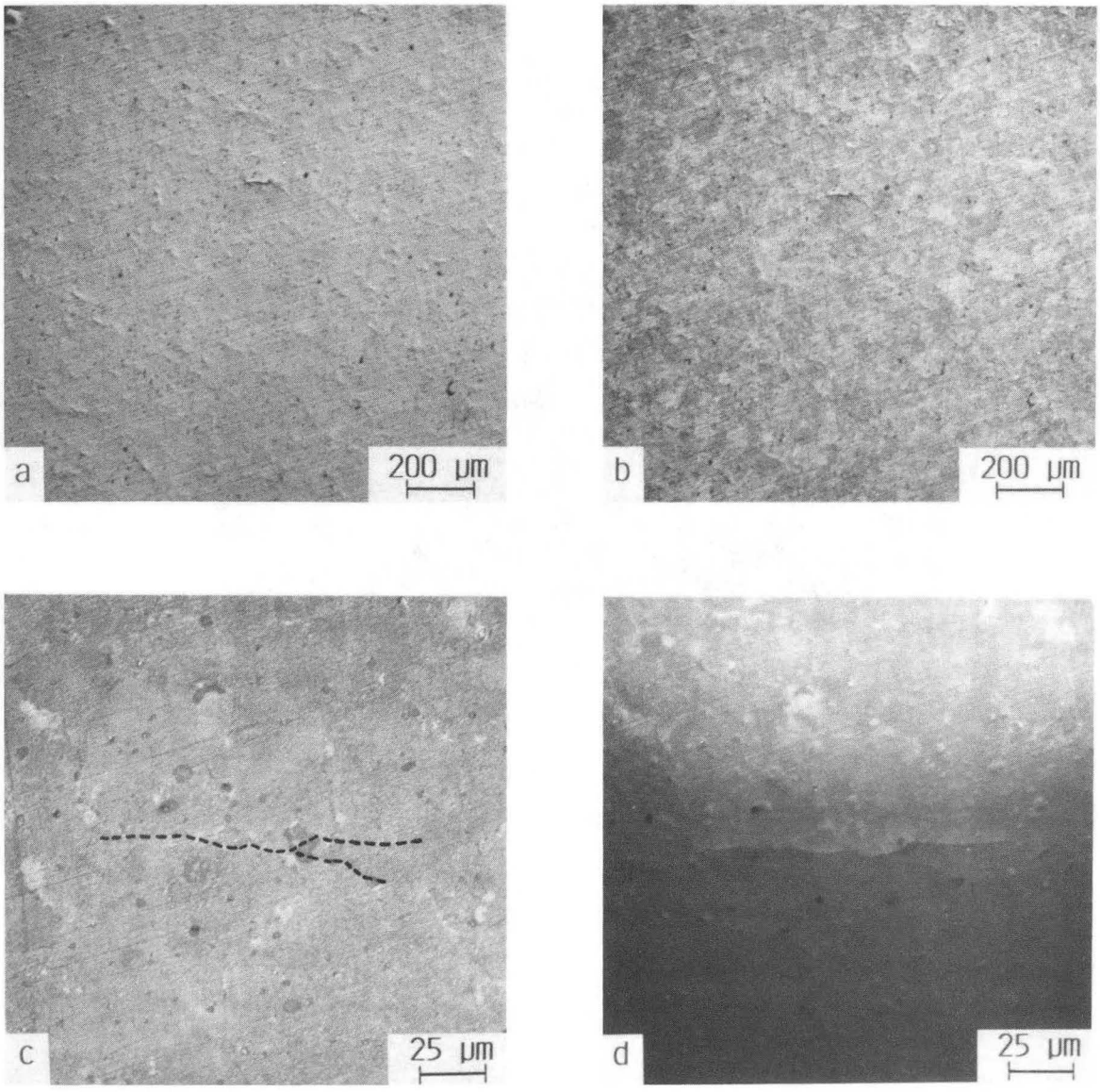

XBB 909-7171

Fig. 6: Detailed optical micrographs showing the morphology of a single microcrack in MS-grade Mg-PSZ following 6900 cycles of tension-compression loading (σ_{max} ~ 450 MPa) (a) using Nomarski interference and (b) with the surface etched in a concentrated HF solution to reveal the underlying microstructure. At higher magnification the microcrack is schematically illustrated in (c) to improve the low contrast with information from (d) which shows the improved contrast obtained from illuminating only one half of the object field.

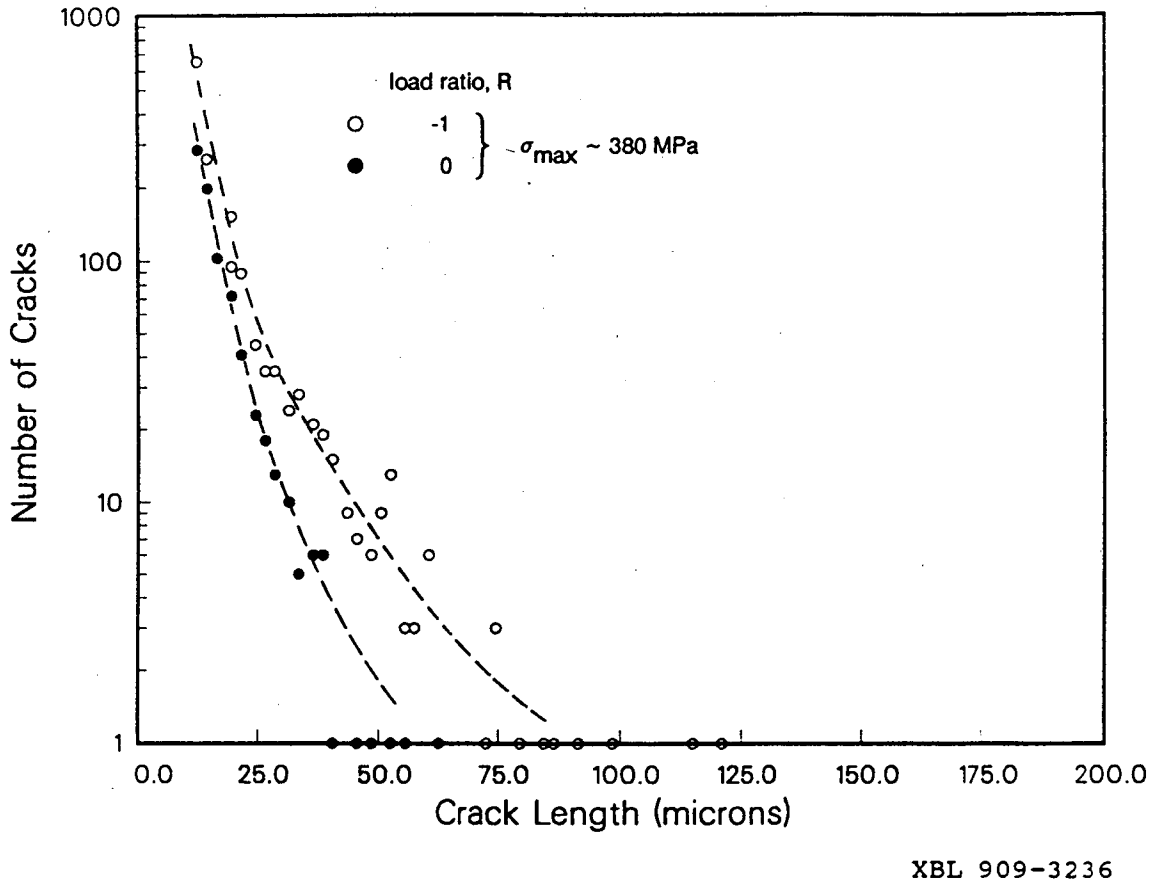

Fig. 7: Microcrack size distributions for MS-grade Mg-PSZ measured on the surface of cantilever-beam specimens at a maximum alternating stress of ~380 MPa for both tension-compression and tension-tension loading.

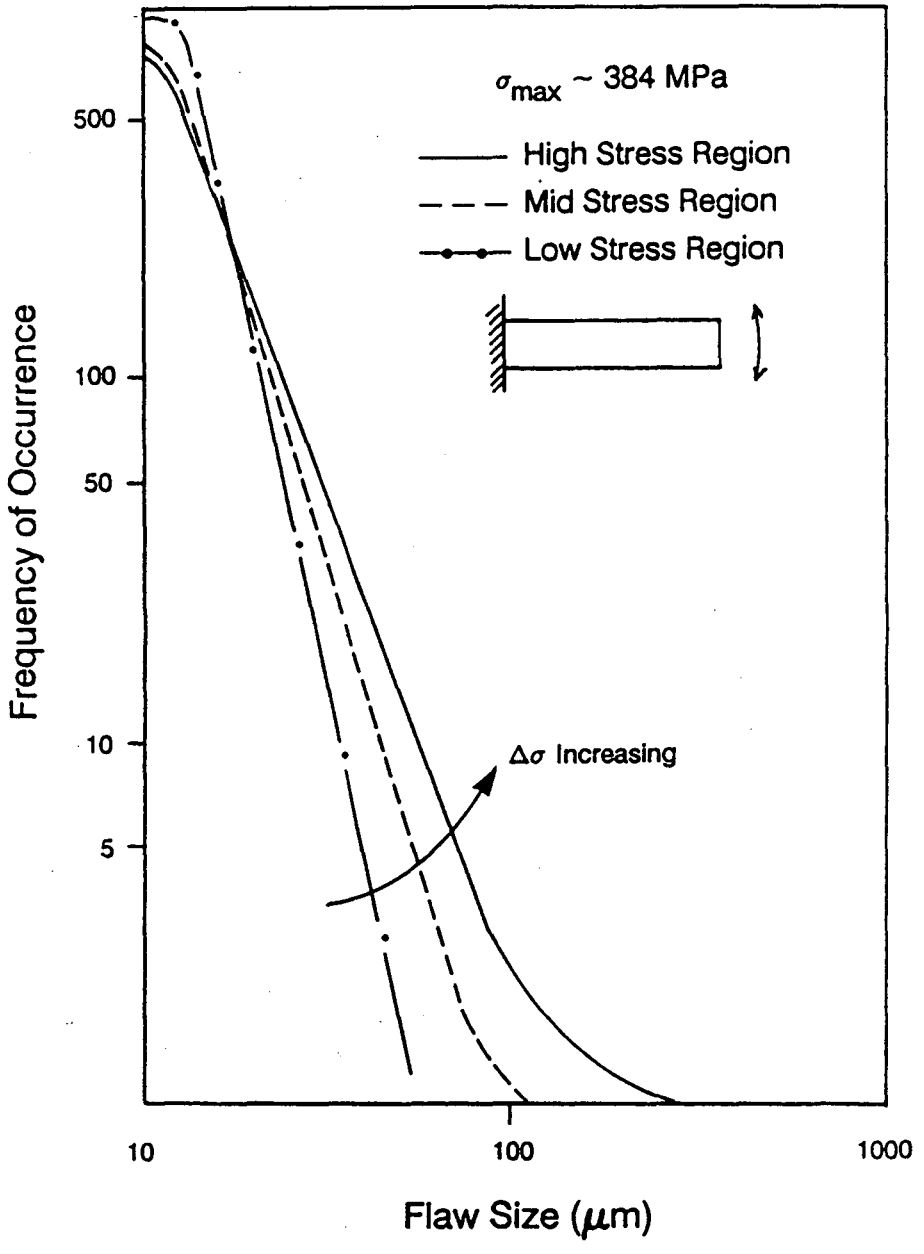

XBL 906-2249A

Fig. 8: Microcrack size distributions after tension-compression loading measured at different locations along the length of the cantilever beam specimens.

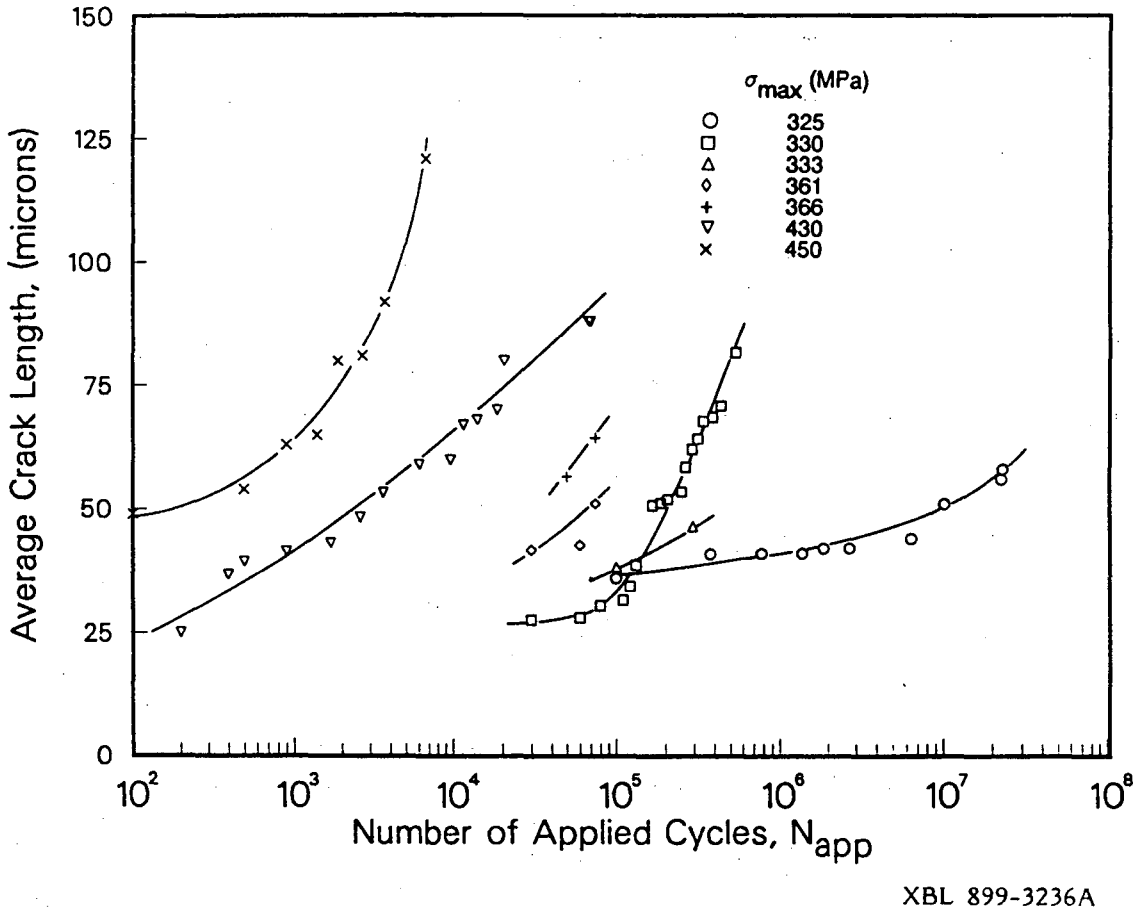

Fig. 9: Crack length vs. number of cycles curves for small-crack growth at various maximum applied stress levels in cantilever-beam specimens of MS-grade Mg-PSZ at R = -1.

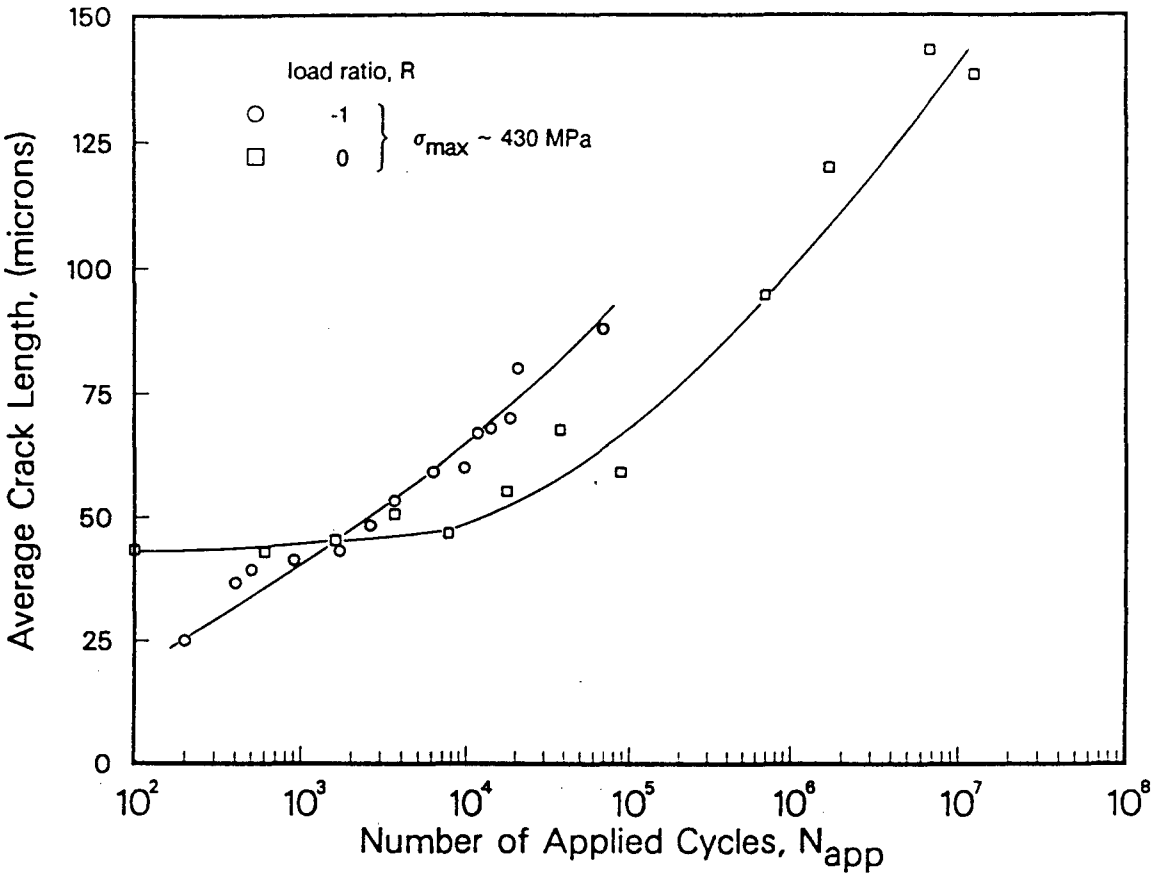

XBL 909-3237

Fig. 10: Crack length vs. number of cycles for small-crack growth at similar applied stress levels in cantilever-beam specimens of MS-grade Mg-PSZ at R = 0 and R = -1.

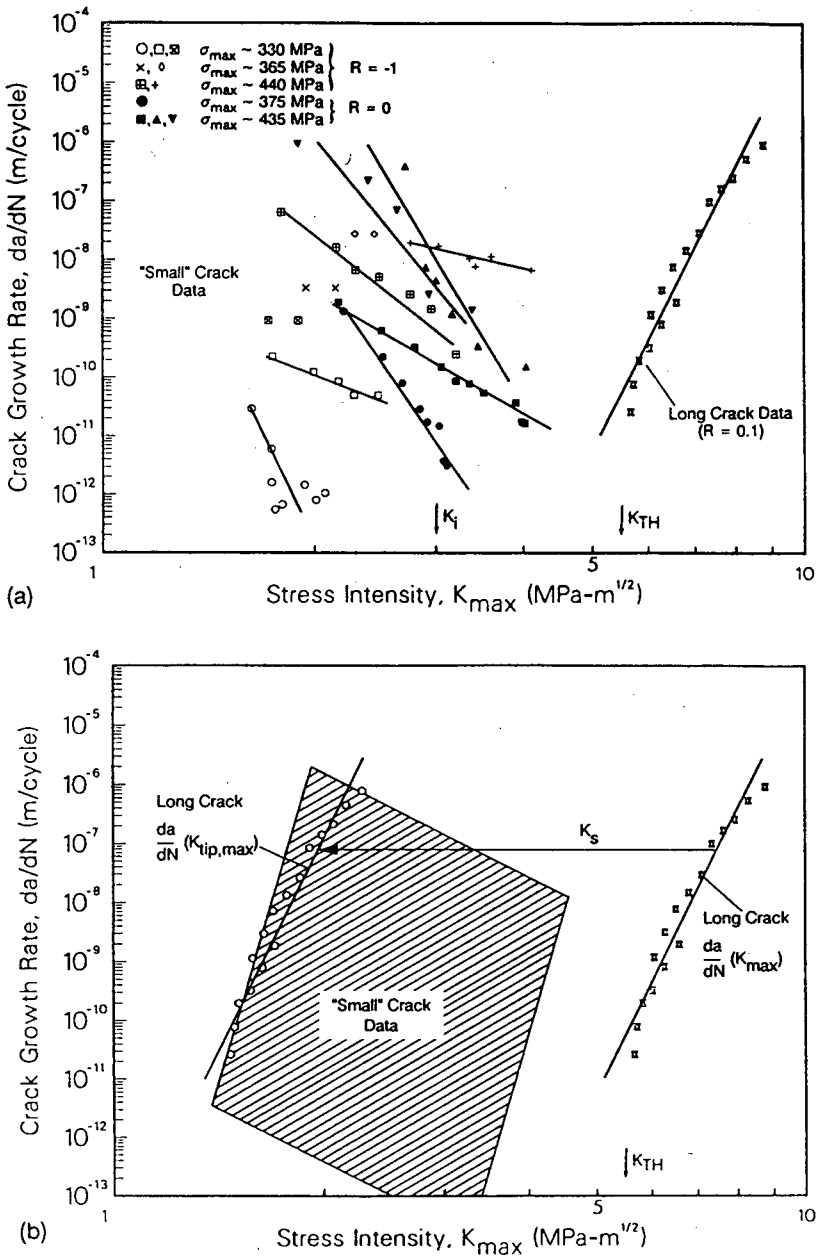

Fig. 11: Small-crack growth-rate data in MS-grade Mg-PSZ from cantilever-beam specimens, as a function of K_{max} at R = 0 and -1, compared to corresponding long-crack data as a function of the maximum applied stress intensity in (a), and (b) showing schematically small-crack data compared to the near-tip stress intensity relationship for the long crack data computed from Eq. 5. Note how small cracks propagate at stress-intensity levels well below the nominal long-crack threshold, ΔK_{TH}, for cyclic crack-growth, and even below the initiation toughness, K_i, for monotonic loading in (a); initial growth, however, occurs at stress intensities typical of unshielded long cracks in (b).

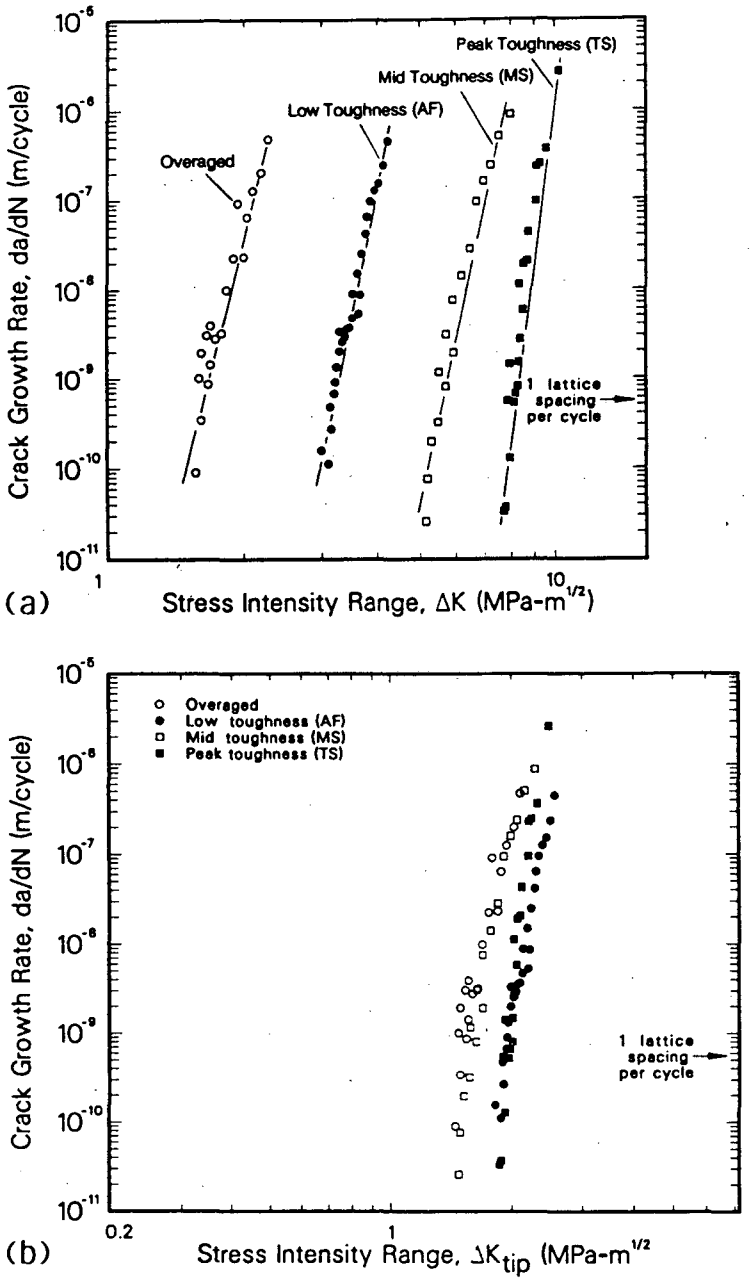

XBL 893-931-A

Fig. 12: Long-crack growth-rate data in overaged and transformation-toughened Mg-PSZ, derived from C(T) specimens, as a function of a) nominal (applied) stress-intensity range, ΔK, and b) near-tip stress-intensity range, $\Delta K_{tip} = K_{max} - K_s$, showing that cyclic crack-growth resistance is increased with the magnitude of transformation toughening.

LAWRENCE BERKELEY LABORATORY
UNIVERSITY OF CALIFORNIA
INFORMATION RESOURCES DEPARTMENT
BERKELEY, CALIFORNIA 94720